THERMODYNAMIC AND NONSTOICHIOMETRIC BEHAVIOR OF PROMISING Hi-Tc CUPRATE SYSTEMS VIA EMF MEASUREMENTS: A SHORT REVIEW*

Marvin Tetenbaum

Chemical Technology Division
Argonne National Laboratory
9700 South Cass Avenue
Argonne, Illinois 60439

To be presented at the Milton Blander International Symposium on "Thermodynamic Predictions and Applications" at the TMS Meeting, February 28-March 4, 1999, San Diego, CA, USA
Submitted for publication in the Transactions of The Metallurgical Society

March 1999

---

*This work was supported by the U.S. Department of Energy, Energy Efficiency and Renewable Energy, as part of a DOE program to develop electric power technology, under Contract W-31-109-ENG-38.

THERMODYNAMIC AND NONSTOICHIOMETRIC BEHAVIOR OF PROMISING Hi-Tc CUPRATE SYSTEMS VIA EMF MEASUREMENTS: A SHORT REVIEW.

Marvin Tetenbaum, Chemical Technology Division, Argonne National Laboratory, 9700 South Cass Avenue, Argonne, Illinois 60439, USA.

ABSTRACT

Electromotive force (EMF) measurements of oxygen fugacities as a function of stoichiometry have been made on the $YBa_2Cu_3O_x$, $GdBa_2Cu_3O_x$, $NdBa_2Cu_3O_x$ and bismuth cuprate systems in the temperature range ~400-750°C by means of an oxygen titration technique with an yttria-stabilized zirconia electrolyte. The shapes of the 400°C isotherms as a function of oxygen stoichiometry for the Gd and Nd cuprate systems suggest the presence of miscibility gaps at values of x that are higher than those in the $YBa_2Cu_3O_x$ system. For a given oxygen stoichiometry, oxygen partial pressures above $GdBa_2Cu_3O_x$ and $NdBa_2Cu_3O_x$ are higher (above x=6.5) than that for the promising $YBa_2Cu_3O_x$ system.

A thermodynamic assessment and intercomparison of our partial pressure measurements with the results of related measurements will be presented.

1. Introduction

This paper will present an overview of experimental studies that were carried out in the Chemical Technology Division at Argonne National Laboratory to investigate the nonstoichiometric and thermodynamic behavior of promising high-Tc cuprate superconductor oxide systems as a function of oxygen partial pressure, oxygen stoichiometry, and temperature via EMF measurements. The systems investigated include 1) the promising $YBa_2Cu_3O_x$ (Y-123) system, 2) related rare-earth systems, $NdBa_2Cu_3O_x$ (Nd-123), and $GdBa_2Cu_3O_x$ (Gd-123), and 3) the bismuth perovskite systems, $Bi_2Sr_2Ca_1Cu_2O_x$ (Bi-2212), and lead-doped $Bi_2Sr_2Ca_2Cu_3O_x$ (Bi-2223). However, this paper will mainly emphasize the results obtained with the Y-123, Nd-123, and Gd-123 systems.

It should be noted that renewed interest in the Y-123 system and related rare-earth RE-123 systems has occured because of promising developments of coated conductors which

DISCLAIMER

DISCLAIMER

Portions of this document may be illegible in electronic image products. Images are produced from the best available original document.

can yield significantly higher current densities in Tesla-level magnetic fields than Bi-2212 and lead-doped Bi-2223 systems.

We have reported previous oxygen partial pressure measurements on the Y-123 and Nd-123 systems [1,2,3,4]. In these studies the oxygen content was varied in well-defined small increments by means of a coulometric titration technique, and the equilibrium partial pressure (fugacity) above the sample was established from EMF measurements [5]. This method is sensitive to detecting phase transformations, oxygen nonstoichiometry, and thermodynamic properties of Y-123 and RE-123 systems, where the single phase homogeneity regions have a wide range of oxygen content in the condensed phase. It should be noted that the coulometric technique has been utilized in promising bismuth-cuprate perovskite systems, where the single-phase homogeneity regions have a very narrow range of oxygen content [6,7,8].

The transition temperatures have been reported to be about 90 K for Y-123, 92 K for Gd-123,and 96 K for Nd-123, where x is close to the value of 7.0, with an oxygen deficiency x=$\sim$6.8. Note that ionic radii of trivalent Y, Gd, and Nd are 0.99, 1.02, and 1.10 Å, respectively [9], and that the transition temperature increases with increase of ionic radius. Between x=6.5 and 7.0, the results of Veal et al. [10] for Y-123 showed two plateaus, one at 60 K and one at 90 K. It was postulated that the 60 K plateau (x=$\sim$6.63-6.80) characterizes the ortho-II structure and the 90 K plateau (x=$\sim$6.80-7.0) characterizes the ortho-I structure. The lower plateau was nearly absent for the case of Nd-123 [10,11].

It should be emphasized that unlike the Y-123 system, solubility of Nd in Ba and Gd in Ba have been observed for the Nd-123 and Gd-123 systems. According to Wu et al. [12] Gd-123 (solid solution) has a solubility limit of x=0.2 in air, and the solubility limit can be reduced in low oxygen partial pressures resulting in precipitation of $GdBa_2CuO_5$ and CuO as second phases. It is thought that these dispersed phases can enhance the Jc of RE-123 type superconductors. However, compositional modulation between Nd and Ba sites in Nd-123 is thought to be the promoter of improved flux pinning for large Jc, rather than the presence

of Nd-422 dispersed in the melt-processed Nd-123 matrix [13].

Our EMF measurements on the Y-123 system will be reviewed in detail because the results of these measurements served as as a basis for investigating other promising Hi-Tc cuprate systems. Limited results of our unpublished measurements on the Gd-123 system will be included in this overview paper.

2. EXPERIMENTAL

The electrochemical cell can be schematically represented by

$$\text{Pt, M } (p(O_2)) \mid ZrO_2(Y_2O_3) \mid \text{Air } (p(O_2)_{ref} = 0.21 \text{ atm}), \text{Pt}$$

where M=the superconductor material under investigation. The equilibrium oxygen partial pressures, $p(O_2)$, above the sample in the cell can be calculated by means of the Nernst equation

$$p(O_2) = p(O_2)_{ref}\ exp\left(-\frac{4EF}{RT}\right)$$

where E is the EMF (open circuit potential) of the cell, F is the Faraday constant, T is the absolute temperature and R is the gas constant.

The oxygen content of the sample under investigation can be varied by means of coulometric titration and calculated from the relationship

$$\Delta n(O_2) = \frac{It}{4F}$$

where $\Delta n(O_2)$ = moles of oxygen transported, I is the controlled current (amps) flowing through the cell for a time t (sec), and F is the Faraday constant. It should be pointed out that yttria-stabilized zirconia has a high mobility of oxygen ions in the lattice of the electrolyte.

The cell used in this study was based on the cell designs described by Tretyakov and Rapp [5], except that soft glass was used as a sealant instead of Pyrex. Pure analyzed air circulating over the cell served as the reference electrode. The cell EMF was measured with a high-impedance electrometer and a Keithley digital voltmeter. Coulometric titrations

were performed with a Princeton Applied Research Model 173 Potentiosat/Galvanostat. The stabilized zirconia electrolyte served as both an oxygen pump and sensor for EMF measurements.

3. Results and Discussion

3.1 Y-Ba-Cu-O System

The samples used for EMF measurements were prepared by the Materials Science Division at the Argonne National Laboratory. The Y-123 sample was received in the form of a ten mil thick sintered tape (~95% theoretical density). The transition temperature was reported to be ~90 K [14]. X-ray examination showed only the orthorhombic structure; oxygen analysis (iodometric titration) gave x=6.891±0.005. The tape was broken up into small granules (sample size, ~30 mg) for use in the EMF measurements.

The results of our EMF measurements are shown in Fig. 1, where equilibrium oxygen pressures calculated for isotherms in the temperature range 400-750°C are plotted as a function of x in $YBa_2Cu_3O_x$. There is no apparent sign of a change in curvature at an oxygen stoichiometry of x~6.5, where the formal valence of copper is two, and where the O-T transition had been assumed to occur by various investigators during the early stages of research on this material.

It is pertinent to point out that upon completion of the run shown in Fig 1, we calculated (based on coulometric titration) that the oxygen content of the residue in the sample holder would be x=6.153. Oxygen analysis of the sample via iodometric titration gave x=6.152±0.005. This agreement gave us confidence in the reliability of the EMF method. In addition, as expected, x-ray examination of the sample in the sample holder showed that the original orthorhomic structure (where x=6.892) was completely transformed to tetragonal.

Of particular importance, the change in curvature of the lower temperature isotherms above x=6.5 shown in Fig. 1 and an inflection around x=6.65 are consistent with the presence of a miscibility gap at lower temperatures. Based on the excellent linear fit, of RT log $p(O_2)$ versus T, we extrapolated values of log $p(O_2)$ versus x, below 400°C [2]. Results indicated

the presence of an orthorhombic-orthorhombic miscibility gap with a consolute temperature of ~200 ±50°C. For the terminal compositions extending between $x = 6.55$ to $x = 6.75$ we estimated a temperature of ~35°C [2].

In addition, a relatively rapid increase of the partial molar entropy of solution of oxygen in $YBa_2Cu_3O_x$ in the composition range x ≅6.75-6.55 (Fig.2) appears to reflect the properties of an orthorhombic-orthorhombic miscibility gap since the extrapolated measurements appear to be completely within the orthorhombic phase field. The increase in $\Delta\bar{S}(O_2)$ with oxygen deficiency in $YBa_2Cu_3O_x$ at x <6.5 is related to the O-T transition and reflects the differences between the distributions of oxygen atoms and vacancies in the relatively disordered tetragonal structure and the more ordered orthorhombic structure.

The presence of a miscibility gap at low temperatures due to two orthorhombic structures has been suggested by a number of theoretical studies. Curtiss et al. [15] postulated a phase diagram based, in part, on semiempirical molecular orbital theory, which suggested two orthorhombic structures in the region x >6.5. They speculated that one of the structures would have fully occupied oxygen chain sites (01), while the other would have partially occupied chain sites. Khachaturyan et al. [16] estimated a phase diagram based on a mean field model and experimental data for the T→O transition. Their calculated diagram predicts a peritectoid decomposition into two phase fields below ~190°C, namely, O′ (where x =6.5) + O_x, or O′ + T. Wille et al. [16] have calculated a phase diagram by application of the cluster variation method to an asymmetric two-dimensional Ising model with interaction parameters selected to guarantee the stability at x =6.5 of the experimentally observed double cell structure. However, their calculated phase-diagram is not consistent with our measurements. Goodenough and Manthiram [17]]have suggested that interchain ordering of the oxygens can give rise to several discrete Magneli-type orthorhombic structures.

3.2 Nd-Ba-Cu-O System

As in the case of Y-123, from plots of equilibrium oxygen pressures versus x, no sign of a change in curvature was obtained at an oxygen stoichiometry of x=6.5, where copper

is divalent, and where the the O-T structural transition had been thought to occur. The results are shown in Fig. 3. The shape of the 400°C isotherm suggests the presence of a miscibility gap at lower temperstures, at values of x that are higher than those in the Y-123 system. The shifts in the location of the miscibility gaps are consistent with the changes of the composition of Tc with ionic radii for Y and Nd in Y-123 and Nd-123. For a given oxygen stoichiometry, partial pressures above Nd-123 were found to be higher than those for Y-123 as reflected in the calculated partial molar quantities $\Delta\overline{S}(O_2)$ and $\Delta\overline{H}(O_2)$. Our results appear to explain the two plateaus in measured values of Tc as a function of oxygen stoichiometry in orthorhombic Y-123, and appear to be consistent with the less pronounced Tc plateaus found for the Nd-123 system at higher values of oxygen stoichiometry.

3.3 Gd-Ba-Cu-O System

Fig. 4 shows a plot of partial pressure of oxygen as a function of temperature and oxygen stoichiometry for Gd-123. It should be noted that extensive EMF measurements were initially made at 600°C in order to establish whether the measurements were reversible with varying oxygen content. As in the case of the Y-123 and Nd-123 systems, the EMF (and thereore the calculated oxygen partial pressures) showed reversible behavior for oxygen absorbtion and desorbtion over the composition range investigated. Temperature dependency measurements of oxygen partial pressure for selected compositions obtained from the coulometric titrations at 600°C were also carried out. The results are included in Fig. 4 (for the 400, 450 and 500°C isotherms). A typical example of the reversible behavior of the temperature dependency of oxygen partial pressure for a given oxygen content is shown in Fig. 5 for x=6.33. Fig. 6 shows an overview plot of the temperature dependencies of oxygen partial pressures for various oxygen content values in the condensed phase of Gd-123 derived from our EMF measurements. It is readily seen that cooling these compositions at a fixed oxygen partial pressure increases the oxygen content of the condensed phase. Note that the absence of breaks in the temperature dependency plots indicate that Gd-123 is stable below the CuO/Cu_2O diphasic equilibrium line based on our measurements in the

temperature range investigated. Oxygen partial pressures above coexisting pure CuO-Cu_2O phases [19] are included in the figures as broken lines. The EMF measurements of Bormann and Nolting [20] show that lead-free Bi-2212 and Y-123 generally decompose very close to the CuO/Cu_2O boundary. Our results with Bi-2212 and lead doped Bi-2223 also indicate decomposition close to the CuO/Cu_2O diphasic boundary [6,7,8]. It should be noted, however, that the TGA measurements of Feenstra et al. [21] on Y-123 thin films indicate that the material is stable to at least one order of magnitude lower pressure than the diphasic CuO/Cu_2O system.

In agreement with the results obtained with the Y-123 and Nd-123 systems [1,2], no apparent change in curvature or discontinuity was observed at an oxygen stoichiometry of x=6.5 where the formal valence is two, and where the orthorhombic-tetragonal transition had been assumed to occur by various investigators during the early stages of research on Y-123 compositions.

Fig. 7 shows a comparison of oxygen partial pressure values as a function of oxygen stoichiometry for Y-123, Gd-123, and Nd-123 cuprate systems at 400°C. For a given oxygen stoichiometry, oxygen partial pressures above Gd-123 and Nd-123 are higher (above x=6.5) than that for the Y-123 system, which appears to reflect the effect of the solubility of the rare earth atoms, Nd and Gd in Ba. According to Shaked et al. [22], the repulsion energy of oxygen atoms in O1 and O5 lattice sites in Nd-123 (and therefore also in Gd-123 O1 and O5 lattice sites) is smaller than in Y-123. This lower repulsion energy apparently stabilizes the orthorhombic structure at higher values of x in Nd-123 and Gd-123 compositions compared to Y-123 as indicated in Fig. 7.

3.4 Bi-Sr-Ca-Cu-O Systems

It should be noted that the Bi-2212 system is important, not only because of its relatively high superconducting transition temperature (ranging from $\sim$ 80-90 K), which makes it attractive for silver-clad composite-type conductors for high-field applications, but also because it serves as an important precursor for the preparation of lead-doped Bi-2223 (Tc

$\sim$ 110 K). Key findings of our measurements on bismuth cuprate systems are (1) single-phase stability regions have a narrow range of oxygen non-stoichiometry and (2) solid state decomposition of lead-free Bi-2212, lead-doped Bi-2212, and lead-doped Bi-2223 can all be represented by the diphasic CuO-Cu_2O system [6,7,8].

SUMMARY

This paper presents thermodynamic properties that can be used to estimate the conditions of stability of the Y, Nd and Gd-123 systems as a function of temperature, oxygen partial pressure, and oxygen stoichiometry of the condensed phases. The results of these measurements can serve as a basis for the optimized preparation and susbsequent behavior of the subject systems. It should be emphasized that control of oxygen content can be an important factor for achieving pinning properties that can result in increased Jc values. Key findings of our measurements are (1) single phase stability regions have a wide range of oxygen stoichiometry for isotherms in the temperature range 400-600°C. (2) For a given oxygen stoichiometry, oxygen partial pressures above Gd-123 and Nd-123 are higher (above x=6.5) than that for the Y-123 system. (3) In contrast to the BiSrCaCuO system and in general accord with the Y-123 system, our measurements show that Gd-123 is stable below the CuO/Cu_2O diphasic equilibrium line at low oxygen partial pressures in the temperature range 400-600°C.

ACKNOWLEDGEMENTS

The author is indebted to J.P Singh, M.T. Lanagan, D.K Finnemore, and M. Xu for supplying the samples used in our EMF measurements. The author is also indebted to I.D. Bloom and R. Kumar for their expert guidance in computer operations. This work was supported by the U.S. Department of Energy, Energy Efficiency and Renewable Energy as part of a DOE program to develop electric power technology, under contract W-31-109-ENG-38.

REFERENCES

1. M.Tetenbaum, B. Tani, B. Czech, and M. Blander, *Physica C.*, 1989, vol. 158, pp. 377-380.
2. M. Tetenbaum, L. Curtiss, B. Czech, B. Tani, and M. Blander, in *Physics and Materials Science of High Temperature Superconductors, NATO ASI Series E.*, 1990, vol. 181, pp. 279-296.
3. M. Tetenbaum, P. Tumidajski, I.D. Bloom, D.L. Brown and M. Blander, in *New Physical Properties in Electronic Materials.*, edited by N. Kirov, J.M. Marshal , and A. Vavrek, World Scientific Publishing Co., 1991, pp. 259-280.
4. M.Tetenbaum, P. Tumidajski, D.L. Brown, and M. Blander, *Physica C.*, 1992, vol. 198, pp. 109-117.
5. Tretyakov and R.A. Rapp, *Trans. Met. Soc. of AIME.*, 1969, vol. 245, pp. 1235-1241.
6. M. Tetenbaum, M. Hash, B.S. Tani J.S. Luo and V.A. Maroni, *Physica C.*, 1995, vol. 249, pp. 396-402.
7. M. Tetenbaum and V.A. Maroni, *Physica C.*, 1996, vol. 260, pp. 71-80.
8. M. Tetenbaum M. Hash, B.S. Tani, and V.A. Maroni, *Physica C.*, 1996, vol 270, pp. 114-128.
9. R.D. Shannon, *Acta Crystallogr.*, 1976, vol. A32, pp. 751-768.
10. B.W. Veal, A.P. Paulikas, J.W. Downey, H. Claus, K. Vandervoort, G. Tomlins, H. Shi, M. Jensen, and L. Morss, *Physica C.*, 1989, vol. 162-164, pp. 97-98.
11. R. Nagarajan, R. Vijayaraghavan, R.A. Mohan Ram, and C.N.R. Rao, *Physica C.*, 1989, vol. 158, pp. 453-457.
12. H. Wu, M.J. Kramer, K.W. Dennis, and R.W. McCallum, *IEEE Transactions on Applied Superconductivity.*, 1997, vol. 7, pp. 1731-1734.
13. S.I. Yoo, N. Sakai, H. Takaichi, T. Higuchi, and M. Murakami, *Appl. Phys. Lett.*, 1994, vol. 65, pp. 633-635.

14. J.T. Singh, private communication.

15. L.A. Curtiss, T.O. Brun, and D.M. Gruen, *Inorg. Chem.*, 1988, vol. 27, pp. 1421-1425.

16. (a) AG. Khachaturyan, S.V. Semenovskaya, J.W. Morris, Jr., *Phys. Rev. B* 1988, vol. 37, pp. 2243-2246. (b) S.G. Khachaturyan, and J.W. Morris Jr., *Phys. Rev. Lett.*, 1990, vol. 64, pp. 76-79.

17. (a) L.T. Wille, A. Berea and D. de Fontaine, *Phys. Rev. Lett.*, 1988, vol. 60, pp. 1065-1068; (b) A. Berea, and D. de Fontaine, *Phys. Rev. B.*, 1989, vol. 39, pp. 6727-6735; (c) D. de Fontaine, M.E. Mann and G. Ceder, *Phys. Rev. Lett.*, 1989, vol. 63, pp. 1300-1303.

18. J.B. Goodenough and A. Manthiram, *Int. J. Mod. Phys.*, 1988, vol. 2, pp. 379-391.

19. R.A Rapp and D.A Shores, in *Solid Electrolyte Cells in Physicochemical Measurements in Metal Research.*, Ed., R.A Rapp, Interscience Publishers, New York 1970, vol. 4, part 2, pp. 159.

20. R. Bormann and J. Nolting, *Physica C.*, 1989, vol.162-164, pp. 81-82.

21. R. Feenstra, T.R. Lindemar, J.D. Budai, and M.D. Galloway, *J. Appl. Phys.*, 1991, vol. 69, pp. 6569-6585.

22. H. Shaked, B.W. Veal, J. Faber Jr., R.L. Hitterman, U. Balachanan, G. Tomlins, H. Shi, L. Morss, and A.P. Paulikas, *Phys. Rev. B.*, 1990, vol. 41, pp. 4173-4180.

FIGURES .

Fig. 1. Variation of oxygen partial pressure with oxygen content and temperature in $YBa_2Cu_3O_x$.

Fig. 2. Partial molar entropy of solution of oxygen in $YBa_2Cu_3O_x$.

Fig. 3. Variation of oxygen partial pressure with oxygen content and temperature. in $NdBa_2Cu_3O_x$.

Fig. 4. Variation of oxygen partial pressure with oxygen content and temperature in $GdBa_2Cu_3O_x$.

Fig. 5. Temperature dependence of partial pressure of oxygen for x=6.33 in Gd-123. (Note reversible behavior).

Fig. 6. Temperature dependence of partial pressure of oxygen with oxygen content (overview plot-$GdBa_2Cu_3O_x$ system).

Fig. 7. Partial pressure of oxygen as a function of oxygen stoichiometry above Gd-123, Nd-123, and Y-123 systems at 400°C.

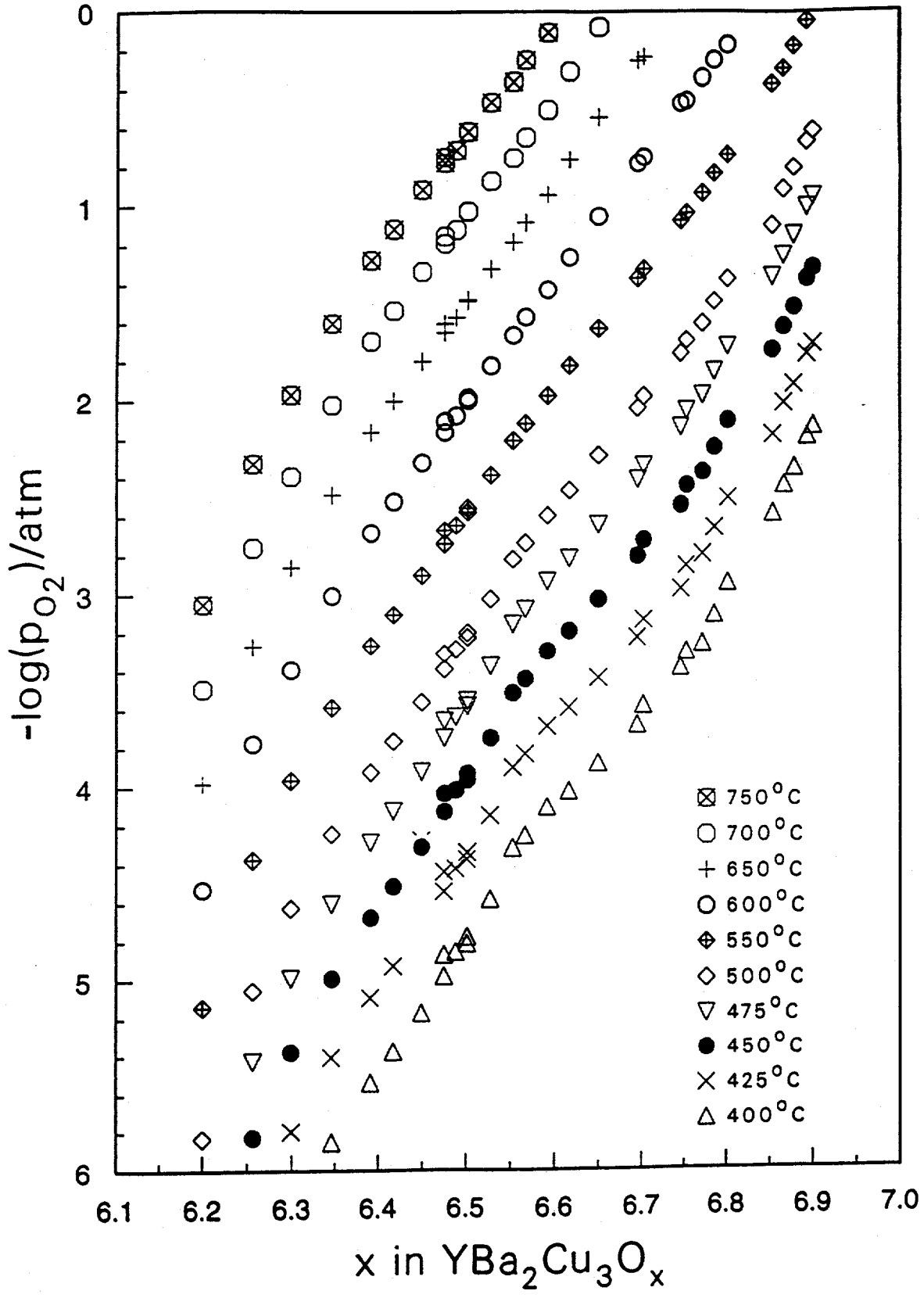
0
1
2
3
4
5
6
-log(p$_{O_2}$)/atm
6.1
6.2
6.3
6.4
6.5
6.6
6.7
6.8
6.9
7.0
x in YBa$_2$Cu$_3$O$_x$
750°C
700°C
650°C
600°C
550°C
500°C
475°C
450°C
425°C
400°C

FIG. 1

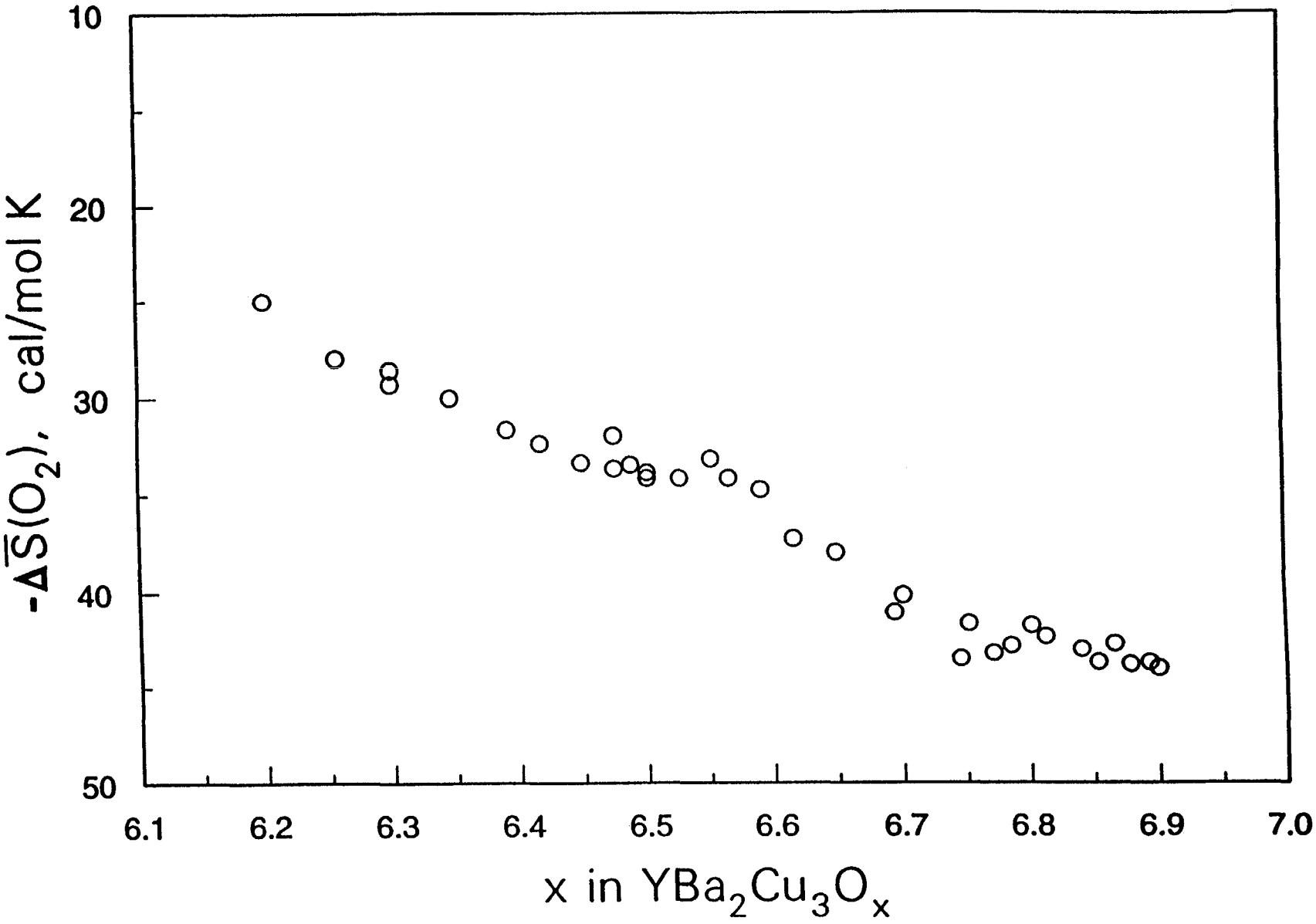
10
20
30
40
50
$-\Delta\bar{S}(O_2)$, cal/mol K
6.1
6.2
6.3
6.4
6.5
6.6
6.7
6.8
6.9
7.0
x in $YBa_2Cu_3O_x$

FIG. 2

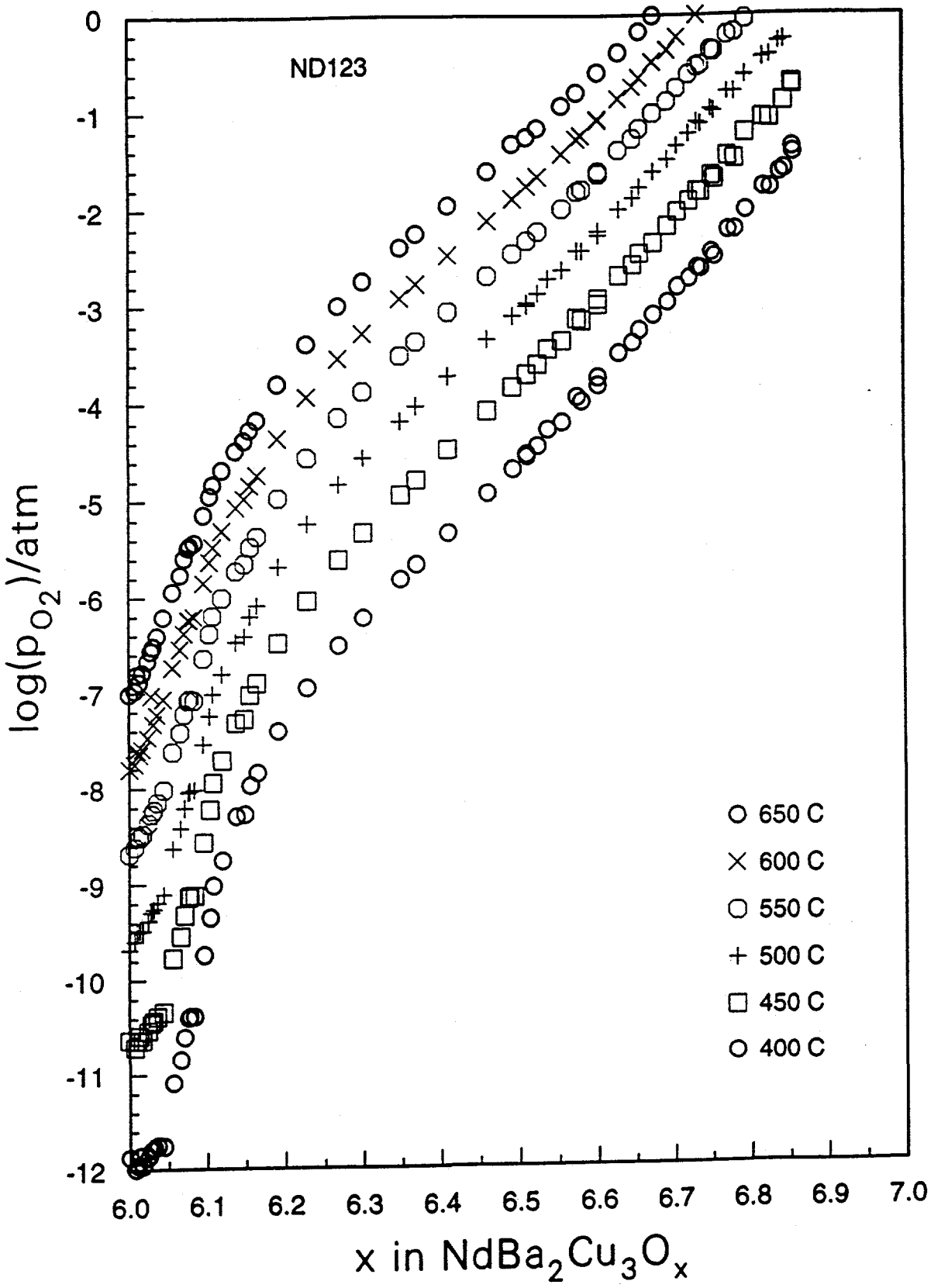
ND123
0
-1
-2
-3
-4
-5
-6
-7
-8
-9
-10
-11
-12
log(p$_{O_2}$)/atm
6.0
6.1
6.2
6.3
6.4
6.5
6.6
6.7
6.8
6.9
7.0
x in NdBa$_2$Cu$_3$O$_x$
650 C
600 C
550 C
500 C
450 C
400 C

Fig. 3

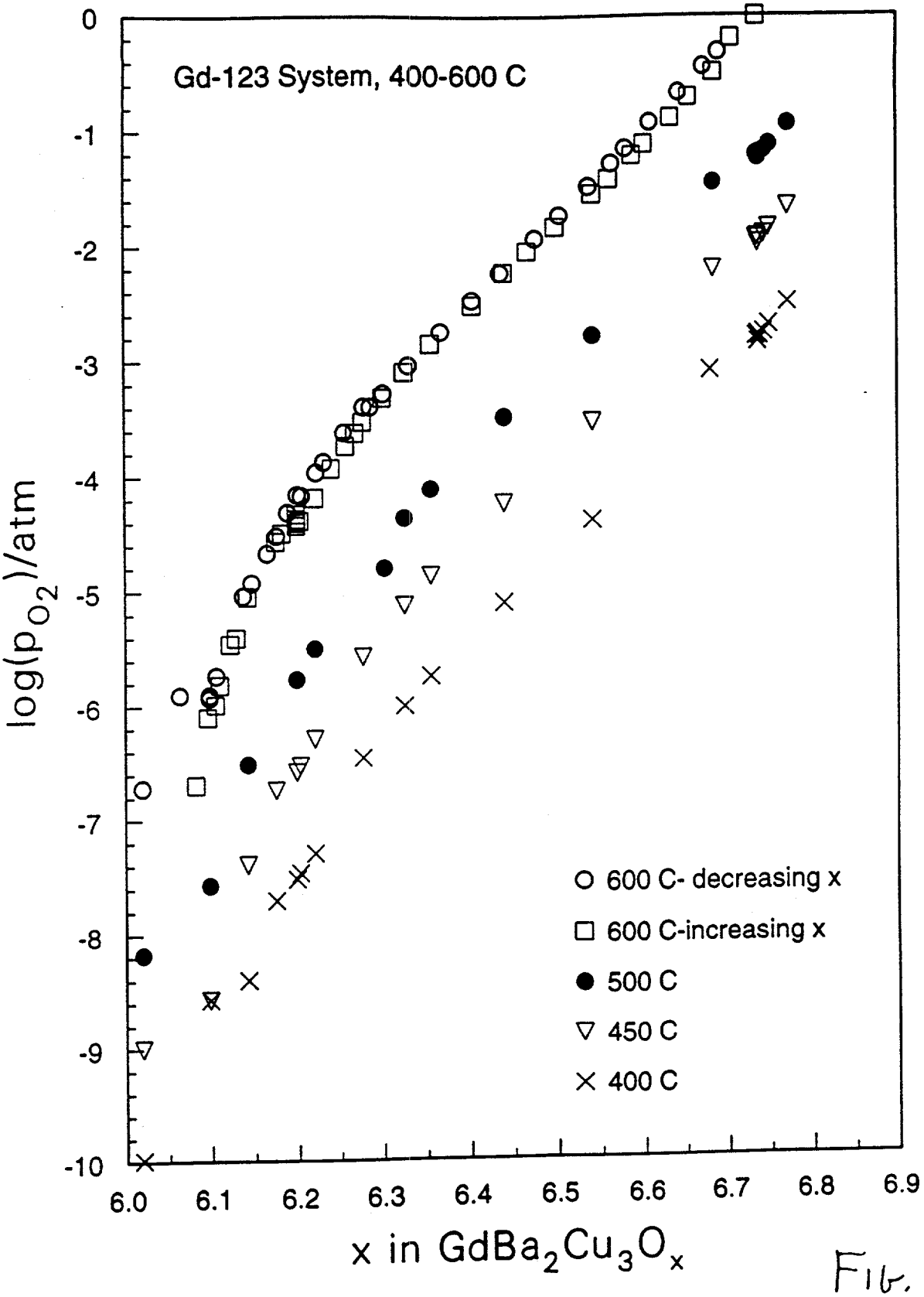
Gd-123 System, 400-600 C
0
-1
-2
-3
-4
-5
-6
-7
-8
-9
-10
log(p$_{O_2}$)/atm
6.0
6.1
6.2
6.3
6.4
6.5
6.6
6.7
6.8
6.9
x in GdBa$_2$Cu$_3$O$_x$
600 C- decreasing x
600 C-increasing x
500 C
450 C
400 C

Fig. 4

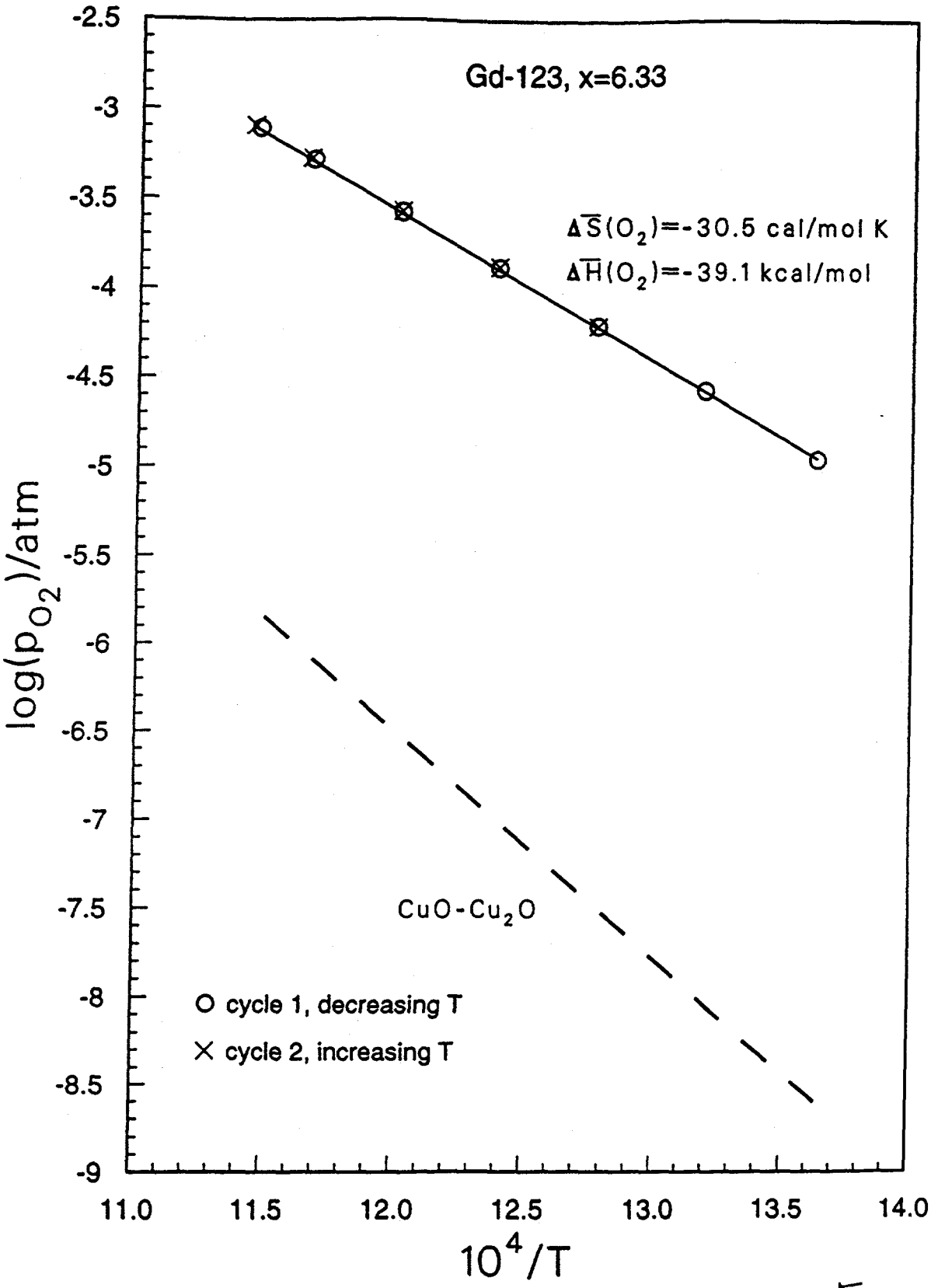
Gd-123, x=6.33
$\Delta\overline{S}(O_2)$=-30.5 cal/mol K
$\Delta\overline{H}(O_2)$=-39.1 kcal/mol
$CuO-Cu_2O$
O cycle 1, decreasing T
× cycle 2, increasing T
$\log(p_{O_2})$/atm
$10^4/T$
-2.5
-3
-3.5
-4
-4.5
-5
-5.5
-6
-6.5
-7
-7.5
-8
-8.5
-9
11.0
11.5
12.0
12.5
13.0
13.5
14.0

FIG. 5

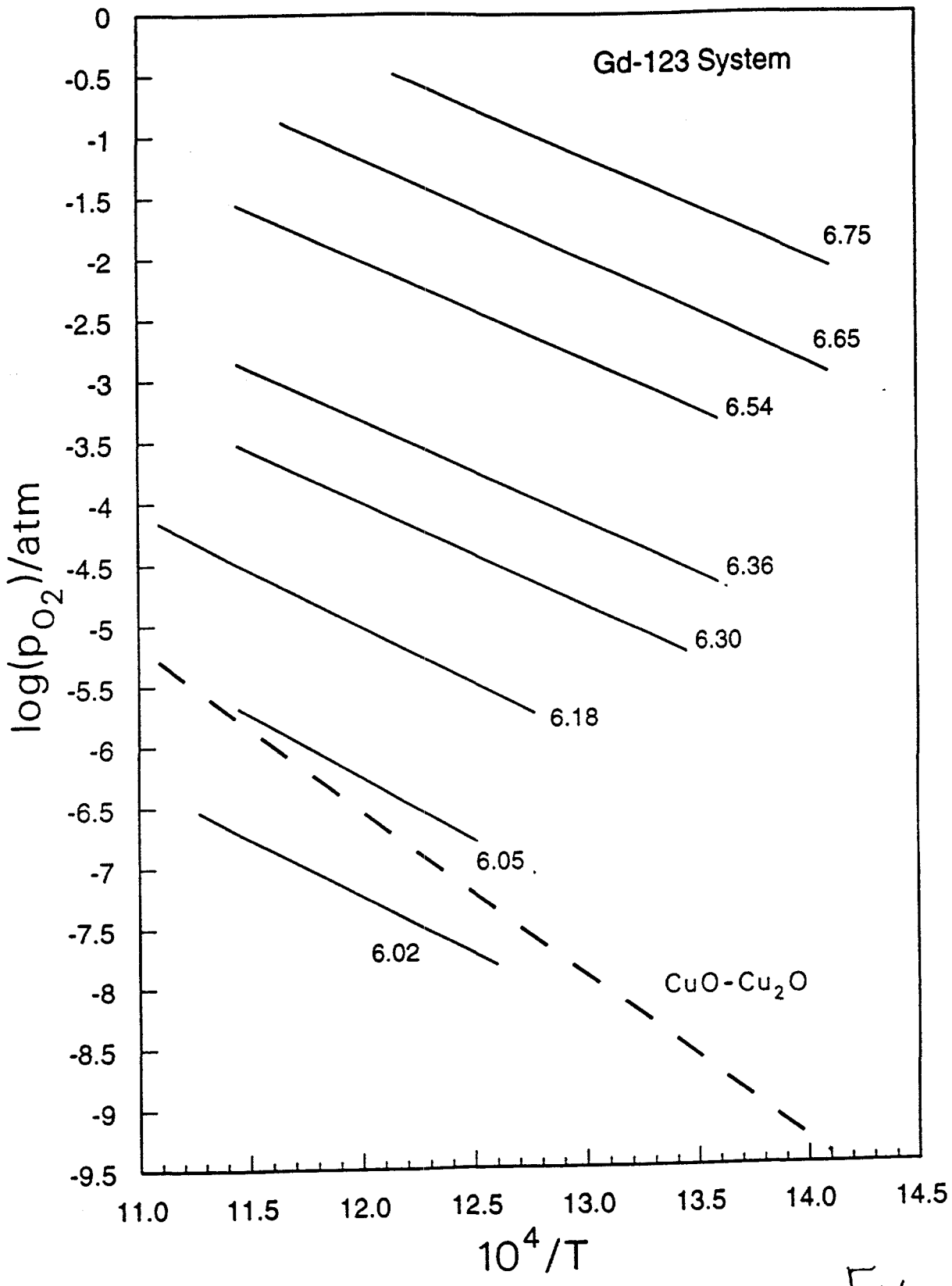
Gd-123 System
6.75
6.65
6.54
6.36
6.30
6.18
6.05
6.02
CuO-Cu2O
log(pO2)/atm
0
-0.5
-1
-1.5
-2
-2.5
-3
-3.5
-4
-4.5
-5
-5.5
-6
-6.5
-7
-7.5
-8
-8.5
-9
-9.5
11.0
11.5
12.0
12.5
13.0
13.5
14.0
14.5
10^4/T

Fig. 6

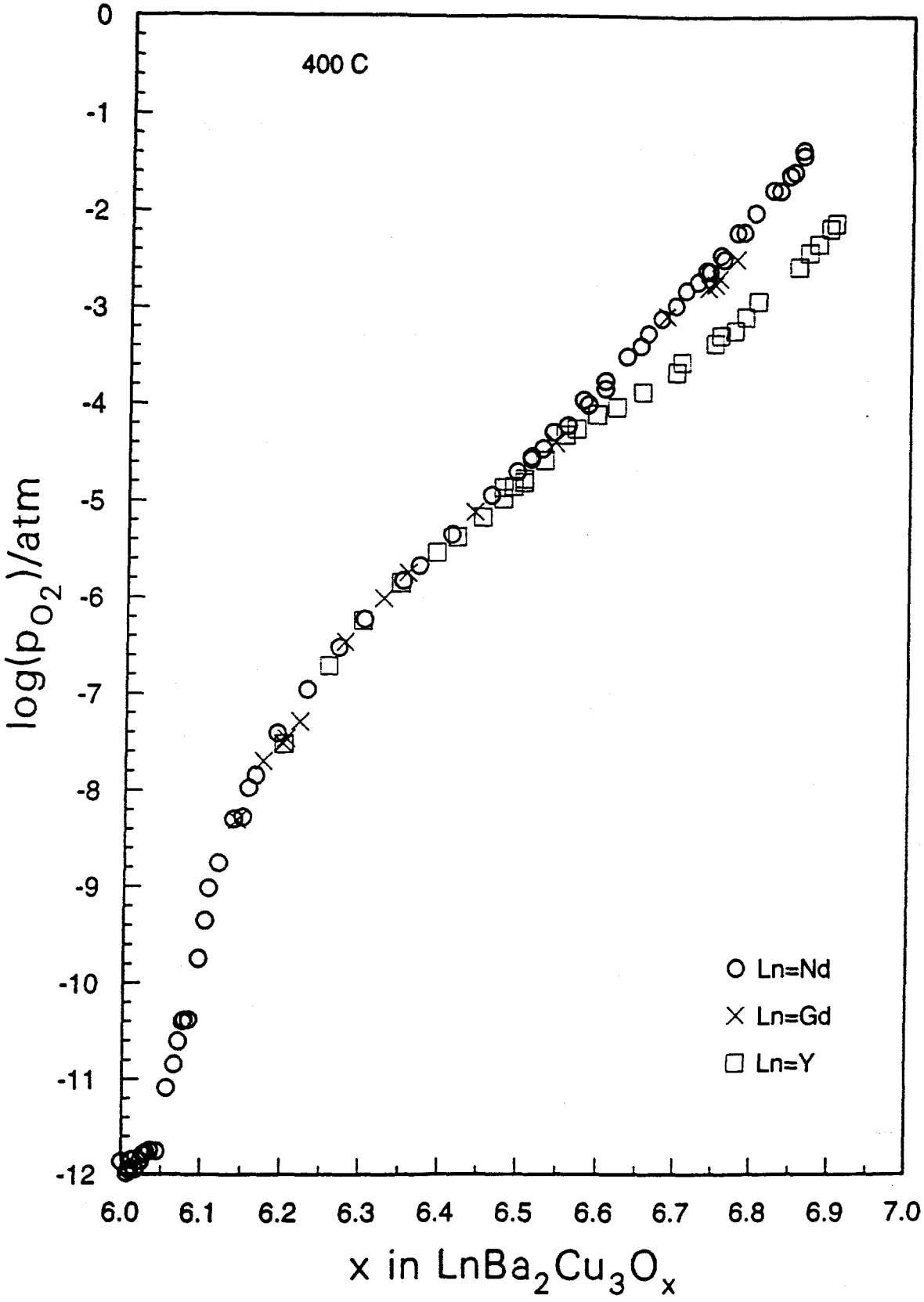
400 C
0
-1
-2
-3
-4
-5
-6
-7
-8
-9
-10
-11
-12
log(p$_{O_2}$)/atm
6.0
6.1
6.2
6.3
6.4
6.5
6.6
6.7
6.8
6.9
7.0
x in LnBa$_2$Cu$_3$O$_x$
O Ln=Nd
× Ln=Gd
□ Ln=Y

Fig. 7